Electron magnetic moment of transient chiral phonons in KTaO3

(article starts on next page)

Letter

Electron magnetic moment of transient chiral phonons in KTaO₃

R. Matthias Geilhufe [1] and Wolfram Hergert[2]

[1]*Department of Physics, Chalmers University of Technology, SE-412 96 Gothenburg, Sweden*
[2]*Institute of Physics, Martin Luther University Halle-Wittenberg, D-06120 Halle, Germany*

High-intensity THz lasers allow for the coherent excitation of individual phonon modes. The ultrafast control of emergent magnetism by means of phonons opens up new tuning mechanisms for functional materials. While theoretically predicted phonon magnetic moments are tiny, recent experiments hint towards a significant magnetization in various materials. To explain these phenomena, we derive a coupling mechanism between the phonon angular momentum and the electron spin. This coupling introduces the transient level splitting of spin-up and spin-down channels and a resulting magnetization. We estimate this magnetization on the example of the lowest infrared active mode in the perovskite KTaO₃. Our results show an electronic magnetic moment of $\approx 10^{-1}$ μ_B per unit cell, depending on the doping level and electron temperature.

Chiral phonons or circularly polarized phonons carry angular momentum [1,2]. As the collective excitation of charged ions, a magnetization occurs. Such a magnetization can be understood in the framework of the dynamical multiferroicity [3] or, more specifically, the phonon inverse Farraday effect [4–7]. However, for a cyclotron motion, comparing the phonon magnetic moment $\mu_{\text{phonon}} = \frac{e\hbar}{2m_{\text{ion}}}$ with the electron magnetic moment $\mu_B = \frac{e\hbar}{2m_e}$, the effect is smaller by a factor of $\frac{m_{\text{ion}}}{m_e}$, i.e., in the range of the nuclear magneton [8,9].

In contrast, recent experiments observed large phonon magnetic moments. In such experiments, optical phonons are excited with a circularly polarized THz laser pulse. Cheng *et al.* measured the phonon Zeeman effect in the Dirac semimetal Cd_3As_2 and observed a moment of ≈ 2.7 μ_B [10]. They explain the giant magnetic moment by a coupling of the phonon to the effective Dirac electron, in resonance with the cyclotron frequency. Baydin *et al.* revealed a phonon Zeeman splitting of similar size in the semiconductor PbTe [11]. Here, the magnetic moment was explained in terms of strong anharmonicity effects. The effect even increases after a topological phase transition in thin films of the related compound $Pb_{1-x}Sn_xTe$ ($x > 0.32$) [12]. Basini *et al.* measured the dynamical magnetization by chiral phonons in $SrTiO_3$ using optical Kerr rotation and, again, found a magnetic moment of similar size [13]. The effect is explained by the angular momentum transfer from phonons to electrons in terms of the inverse Barnett effect and a resulting enhanced gyromagnetic ratio.

The mismatch of theory and experiment gives evidence that phonons cannot be described in the absence of electrons. Instead, electron-phonon and, specifically, spin-phonon coupling play a significant role in explaining the emergent dynamical magnetization. Mechanisms for interactions of the lattice and spins have been known for a long time, e.g., from the early work of Elliot and Yafet on spin relaxation [14,15], and have let to sophisticated *ab initio* implementations [16]. Generally, the coupling of lattice degrees of freedom to the spin requires spin-orbit interaction and can be modeled by assuming small atomic displacements in the potential energy [17]. Other approaches are based on modifications in the magnetic exchange [18,19] or an inverse Katsura-Nagaosa-Balatsky mechanism [20–22]. To incorporate an additional orbital magnetization, Ren *et al.* [23] showed that the second Chern form times the phonon angular momentum gives rise to a magnetization, in the framework of the modern theory of magnetization [24–26]. Additionally, a nonzero phonon angular momentum might also induce dynamical coupling terms based on quantum inertial effects [27], similar to the expected spin-rotation coupling in mechanical resonators inducing acoustic phonons [28–30]. The expected size of a dynamical magnetization due to spin-rotation coupling will be discussed throughout this Letter.

For simplicity, we consider a twofold degenerate phonon mode $\boldsymbol{q} = (q_1, q_2)$ (in units Å$\sqrt{u}$, with u the atomic mass unit) with eigenfrequency ω_0. The phonon Lagrangian is given by [3]

$$\mathcal{L}^{\text{phonon}}(\boldsymbol{q}, \dot{\boldsymbol{q}}) = \frac{\dot{\boldsymbol{q}}^2}{2} - \frac{\omega_0^2 \boldsymbol{q}^2}{2}. \tag{1}$$

The electron Lagrangian of a nonrelativistic electron in a nominally nonmagnetic material and in the absence of external electromagnetic fields is given by

$$\mathcal{L}^{\text{electron}}(\boldsymbol{\Psi}, \boldsymbol{\Psi}^\dagger) = \int d^3r \left[i\hbar \boldsymbol{\Psi}^\dagger \dot{\boldsymbol{\Psi}} - \boldsymbol{\Psi}^\dagger \left(\frac{\hat{\boldsymbol{p}}^2}{2m} + V(\boldsymbol{r}) \right) \boldsymbol{\Psi} \right]. \tag{2}$$
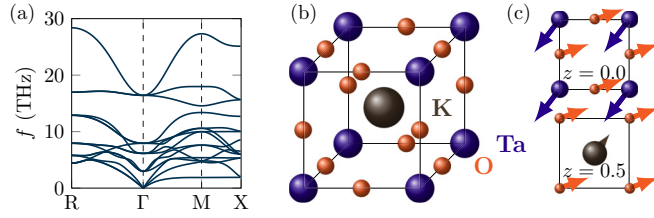
FIG. 1. Phonons in KTaO$_3$. (a) Full phonon spectrum, (b) crystal structure, and (c) eigenvector of the lowest infrared active mode.

We formulate the spin-phonon coupling term with symmetry arguments by considering the two fundamental symmetries time reversal $\mathcal{T}$ and spatial inversion or parity $\mathcal{P}$. The phonon mode $\boldsymbol{q}$ describes the displacement of ions from their equilibrium position. As a result, it transforms as a vector, being odd under $\mathcal{P}$ and even under $\mathcal{T}$. It follows that the time derivative $\dot{\boldsymbol{q}}$ is odd under both $\mathcal{P}$ and $\mathcal{T}$. This is consistent with the transformation behavior of the phonon angular momentum $\boldsymbol{L}^{\text{phonon}} = \boldsymbol{q} \times \dot{\boldsymbol{q}}$, being a pseudovector, i.e., even under $\mathcal{P}$ and odd under $\mathcal{T}$. The same holds for the electron total angular momentum $\boldsymbol{J}^{\text{electron}} = \boldsymbol{L}^{\text{electron}} + \boldsymbol{S}^{\text{electron}}$, with $\boldsymbol{L}^{\text{electron}}$ being the orbital angular momentum and $\boldsymbol{S}^{\text{electron}}$ the spin. Hence, we can write down a $\mathcal{P}$ and $\mathcal{T}$ invariant scalar,

$$\mathcal{L}^{\text{coupl.}} = -\alpha \boldsymbol{L}^{\text{phonon}} \cdot \langle \boldsymbol{J}^{\text{electron}} \rangle, \tag{3}$$

with α being a coupling constant in units of the inverse of the moment of inertia. Note that we use a semiclassical approach here, with the phonon dynamics described classically. This is because we assume a nonequilibrium state with strong phonon amplitude. Hence, the phonon angular momentum is an actual angular momentum [31], as described towards the end of Ref. [32]. By expressing the phonon angular momentum in terms of the angular velocity $\boldsymbol{\omega}^{\text{phonon}}$ and the moment of inertia I, Eq. (3) can be brought into the form of the spin-rotation coupling discussed in Refs. [27–30], $\mathcal{L}^{\text{coupl.}} = \boldsymbol{\omega}^{\text{phonon}} \cdot \langle \boldsymbol{J}^{\text{electron}} \rangle = -I^{-1} \boldsymbol{L}^{\text{phonon}} \cdot \langle \boldsymbol{J}^{\text{electron}} \rangle$. The moment of inertia is given by $I = \int d\boldsymbol{r} r^2 m(\boldsymbol{r})$, with $m(\boldsymbol{r})$ the mass density.

We continue by evaluating the spin-rotation coupling on the example of KTaO$_3$. The phonon dynamics is described using classical equations of motion and coupling the twofold degenerate phonon normal mode $\boldsymbol{q}$ to a circularly polarized THz laser pulse $\tilde{\boldsymbol{E}}(t)$,

$$\ddot{\boldsymbol{q}}(t) + \eta \dot{\boldsymbol{q}}(t) + \omega_0^2 q_i(t) = \tilde{Z} \tilde{\boldsymbol{E}}_0(t). \tag{4}$$

Here, η is the damping or line width and ω_0 is the mode frequency. We focus on the temperature-dependent soft mode, which at 300 K has $\omega_0 = 2.42$ and $\eta = 0.64$ [33]. $\tilde{Z}$ is the mode effective charge. For KTaO$_3$ it takes the value $\tilde{Z} = 1.4$ [9]. For the pulse, we assume $\tilde{\boldsymbol{E}} = \tilde{\boldsymbol{E}}_0 \exp(\frac{1}{2} \frac{(t-t_0)^2}{\tau})[\sin(2\pi\omega t), \cos(2\pi\omega t)]$. $\tilde{\boldsymbol{E}}_0 = \epsilon_\infty^{-1} E_0$ is the screened field strength with $\epsilon_\infty = 4.3$ [34], where we choose $E_0 = 1 \, \text{MV cm}^{-1}$. The pulse width is chosen to be $\tau = \sqrt{\frac{1}{2}}$ ps. For simplicity, we neglect higher-order couplings [35].

The full phonon spectrum of KTaO$_3$ as well as one eigenvector of the soft mode are shown in Fig. 1. The other two eigenmodes are obtained by applying cubic symmetries. The eigenvectors and phonon spectrum have been obtained using density functional perturbation theory [36,37] as implemented
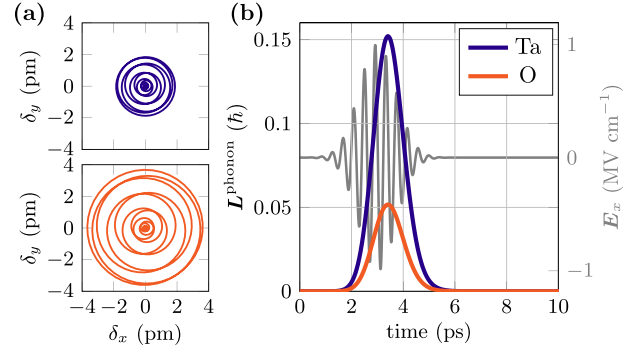
in VASP [38] and PHONOPY [39]. The exchange-correlation functional was approximated by the generalized gradient approximation according to Perdew, Burke, and Ernzerhof [40]. We used a $\boldsymbol{k}$-mesh density of $\approx$1050 $\boldsymbol{k}$ points/Å^{-3}, i.e., an $8 \times 8 \times 8$ mesh and a cutoff energy of 700 eV.

The numerical solution of Eq. (4) is shown in Fig. 2. We focus on O and Ta, as they are the relevant atoms in the electronic structure discussed below. The largest displacement from the atomic equilibrium position is shortly after the pulse peak at 3 ps. The large damping of the phonon makes a distinction from the inverse Faraday effect, i.e., the DC magnetization of a sample exposed to circularly polarized light, challenging. The inverse Faraday effect originates from the time-reversal symmetry breaking due to the photon angular momentum, a term which couples to the magnetic field in the free energy [41]. In contrast, the phonon inverse Faraday effect emerges due to circularly polarized phonons and does not require the presence of an external electric field. Instead, a magnetization is also predicted for thermally excited chiral phonons [42–44].

The electronic structure of KTaO$_3$ is modeled in a two-center Slater-Koster tight-binding scheme [45,46] as implemented in the *Mathematica* group theory package GTPack [47,48] (cf. Appendix). The band structure close to the Fermi energy is plotted in Fig. 3(a). The valence bands are mainly
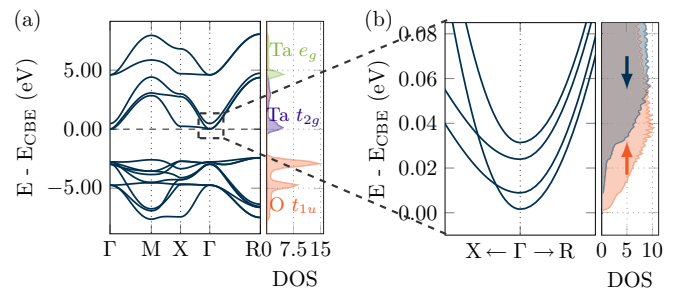

FIG. 2. Calculated atomic motion of oxygen and tantalum in the damped circularly polarized phonon excitation. (a) Displacement $\boldsymbol{\delta}$; (b) site-resolved phonon angular momentum and laser pulse in resonance with the lowest infrared active mode of KTaO$_3$. The damping is $\eta = 0.1 \times 2\pi$ THz.

FIG. 3. Electronic structure of KTaO$_3$ relative to the conduction band edge (E_{CBE}). (a) Full band structure. (b) Expected band splitting of the conduction band due to spin-rotation coupling close to the Γ point. The DOS is projected on the spin-up and spin-down channels.
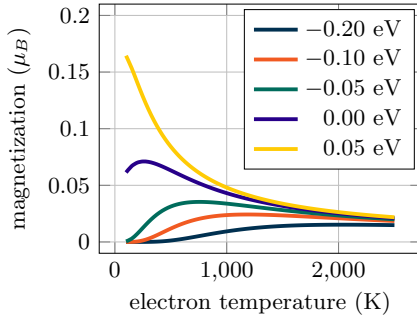
FIG. 4. Electronic magnetization due to spin-phonon interaction. Estimates are given for various values of the chemical potential, relative to the conduction band minimum.

composed of the O-p orbitals, whereas the conduction band is dominated by contributions from Ta-d orbitals. The splitting into t_{2g} and e_g bands due to cubic symmetry is clearly revealed. The band gap is ≈ 2.8 eV and lower than the experimentally observed optical band gap of ≈ 3.6 eV [49]. The splitting of the t_{2g} band at Γ due to spin-orbit interaction is ≈ 0.46 eV.

In the presence of transient chiral phonons, the time-reversal symmetry of the system is broken. As a result, Kramers degeneracy of the electronic bands is lifted. To model this scenario, the tight-binding Hamiltonian is extended by the spin-phonon coupling of Eq. (3). We choose $I^{-1}\boldsymbol{L}^{\text{phonon}} = \boldsymbol{\omega}$ [27], with $\boldsymbol{\omega}$ being the angular velocity of the site-resolved displacement having the frequency $\omega_0 = 2.42 \times 2\pi$ THz. The corresponding coupling to the total angular momentum of the electron, $\boldsymbol{\omega} \cdot \boldsymbol{J}$, is diagonal in the $|j, \mu\rangle$ basis. We project the resulting band structure onto the spin-up and spin-down channels, as shown in Fig. 3(b). We calculate the magnetization by

$$M_z = \mu_B(N_\uparrow - N_\downarrow), \; N_\sigma = \int_{-\infty}^{\infty} dE \, n_\sigma(E) f(E, \mu, T), \quad (5)$$

with $n_\sigma(E)$ the electronic density of states of spin σ and $f(E, \mu, T)$ the Fermi-Dirac distribution. The magnetization (5) is computed with the tight-binding band structure in Fig. 3(b). The dynamically induced magnetization is shown in dependence of the chemical potential μ and electron temperature T in Fig. 4. As can be seen, an electronic magnetization of $\approx 10^{-1} \mu_B$ can be achieved. This moment is about three orders of magnitude larger than the estimate for a purely ionic effect in KTaO$_3$ [8].
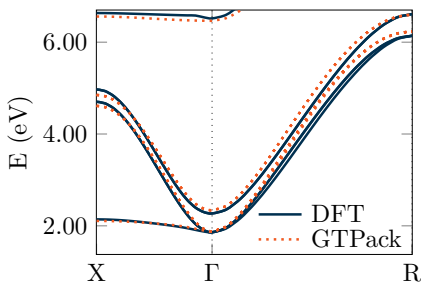
In the estimates, we focus on the chemical potential close to the conduction band edge. In fact, intrinsic doping in KTaO$_3$ crystals, e.g., due to O vacancies, induces subgap states originating from the d electrons of Ta atoms close to the O vacancy [50,51]. While a natural amount of doping ($<10^{18}$ charge carriers/cm^3) still leads to an insulating behavior, a larger amount of O vacancies can induce a metallic state [52]. In the insulating state, a fairly large magnetization occurs if the electronic temperature becomes high. Such a situation might occur for short durations after the crystal was exposed to the laser light [53,54]. Due to the reduced mass of electrons compared to ions, the kinetic energy will be significantly larger until it relaxes into an equilibrium state together with the ions. In contrast, if the Fermi level slightly cuts the conduction band, a lower electronic temperature would be required to exclude contributions to the magnetization from the minority spin channel. Also, we note that electrons can be excited from the subgap states into the conduction band by a multiphoton process in intense laser fields. For low photon energy THz fields, the photon density is significantly higher, making a multiphoton process more likely. Also, such a mechanism can lead to the formation of excitons and induce the transient shift of the chemical potential for electrons and holes.

In summary, we estimated the effect of the chiral spin-phonon coupling $\sim \boldsymbol{L}^{\text{phonon}} \cdot \boldsymbol{J}^{\text{electron}}$. This mechanism induces a split of electronic spin states in the adiabatic approximation. As a consequence, a mismatch of occupied spin-up and spin-down states leads to an emergent magnetization of the order of $10^{-1} \mu_B$. Hence, the effect is larger than the purely ionic phonon inverse Faraday effect by three orders of magnitude. The chiral spin-phonon coupling might be relevant to explain the large experimentally observed phonon magnetic moments due to chiral phonons in various materials [10–13]. Furthermore, also the opposite effect, i.e., the transfer of electronic angular momentum to the lattice, can be described by the chiral spin-phonon coupling and would contribute, e.g., to ultrafast demagnetization effects [31,55,56].

APPENDIX

We construct the tight-binding Hamiltonian using the Slater-Koster scheme [45,46] as implemented in the *Mathematica* group theory package GTPack [47,48]. A restricted basis set containing O p-orbitals and Ta d-orbitals is used. Spin-orbit coupling of Ta d-orbitals is included. The Hamiltonian in the two-center approximation considers nearest-neighbor interactions of Ta and nearest- and

FIG. 5. Comparison of the DFT band structure and the two-center tight-binding band structure using GTPack.

TABLE I. Tight-binding parameters of the Hamiltonian.

$(dd\sigma)_1^{Ta,Ta}$	$(dd\pi)_1^{Ta,Ta}$	$(dd\delta)_1^{Ta,Ta}$	$(pp\sigma)_1^{O,O}$	$(pp\pi)_1^{O,O}$	$(pp\sigma)_2^{O,O}$	$(pp\pi)_2^{O,O}$
0.11409	−0.24820	0.02087	0.38702	−0.0955	0.14458	−0.042634
$(pd\sigma)_1^{O,Ta}$	$(pd\pi)_1^{O,Ta}$	$(dd0)_{t2g}^{Ta}$	$(dd0)_{eg}^{Ta}$	$(pp0)_\perp^{O}$	$(pp0)_\parallel^{O}$	ξ
−2.77242	1.57614	3.08778	6.15932	−1.4078	−2.44059	0.28868

next-nearest-neighbor interactions of O. The Hamiltonian is represented by a 28×28 matrix and contains 14 parameters (see Table I). The crystal field splitting for the on-site parameters is taken into account.

The tight-binding Hamiltonian is fitted to the band structure data obtained using density functional theroy (computational details given in the main text). We refine an initial guess

by the least-squares method. Fifteen k points are taken along each symmetry line. To avoid the algorithm getting stuck in a local minimum in parameter space, we add noise to the parameters after a first step and repeat the minimization scheme. The final result is shown in Fig. 5. It can be seen that the relevant conduction band is well parametrized close to the Γ point.

[1] L. Zhang and Q. Niu, Angular Momentum Of Phonons and The Einstein–de Haas Effect, Phys. Rev. Lett. **112**, 085503 (2014).

[2] A. McLellan, Angular momentum states for phonons and a rotationally invariant development of lattice dynamics, J. Phys. C **21**, 1177 (1988).

[3] D. M. Juraschek, M. Fechner, A. V. Balatsky, and N. A. Spaldin, Dynamical multiferroicity, Phys. Rev. Mater. **1**, 014401 (2017).

[4] D. M. Juraschek, T. c. v. Neuman, and P. Narang, Giant effective magnetic fields from optically driven chiral phonons in $4f$ paramagnets, Phys. Rev. Res. **4**, 013129 (2022).

[5] D. M. Juraschek, D. S. Wang, and P. Narang, Sum-frequency excitation of coherent magnons, Phys. Rev. B **103**, 094407 (2021).

[6] D. M. Juraschek, P. Narang, and N. A. Spaldin, Phonomagnetic analogs to optomagnetic effects, Phys. Rev. Res. **2**, 043035 (2020).

[7] Yu. T. Rebane, Faraday effect produced in the residual ray region by the magnetic moment of an optical phonon in an ionic crystal, Zh. Eksp. Teor. Fiz. **84**, 2323 (1983).

[8] R. M. Geilhufe, V. Juričić, S. Bonetti, J.-X. Zhu, and A. V. Balatsky, Dynamically induced magnetism in KTaO₃, Phys. Rev. Res. **3**, L022011 (2021).

[9] D. M. Juraschek and N. A. Spaldin, Orbital magnetic moments of phonons, Phys. Rev. Mater. **3**, 064405 (2019).

[10] B. Cheng, T. Schumann, Y. Wang, X. Zhang, D. Barbalas, S. Stemmer, and N. Armitage, A large effective phonon magnetic moment in a Dirac semimetal, Nano Lett. **20**, 5991 (2020).

[11] A. Baydin, F. G. G. Hernandez, M. Rodriguez-Vega, A. K. Okazaki, F. Tay, G. T. Noe, I. Katayama, J. Takeda, H. Nojiri, P. H. O. Rappl, E. Abramof, G. A. Fiete, and J. Kono, Magnetic Control Of Soft Chiral Phonons In PbTe, Phys. Rev. Lett. **128**, 075901 (2022).

[12] F. G. Hernandez, A. Baydin, S. Chaudhary, F. Tay, I. Katayama, J. Takeda, H. Nojiri, A. K. Okazaki, P. H. Rappl, E. Abramof *et al.*, Chiral phonons with giant magnetic moments in a topological crystalline insulator, arXiv:2208.12235.

[13] M. Basini, M. Pancaldi, B. Wehinger, M. Udina, T. Tadano, M. C. Hoffmann, A. V. Balatsky, and S. Bonetti, Terahertz electric-field driven dynamical multiferroicity in SrTiO₃, arXiv:2210.01690.

[14] R. J. Elliott, Theory of the effect of spin-orbit coupling on magnetic resonance in some semiconductors, Phys. Rev. **96**, 266 (1954).

[15] Y. Yafet, g Factors and Spin-Lattice Relaxation of Conduction Electrons, in *Solid State Physics*, Vol. 14, edited by F. Seitz and D. Turnbull (Academic Press, 1963).

[16] J. Fransson, D. Thonig, P. F. Bessarab, S. Bhattacharjee, J. Hellsvik, and L. Nordström, Microscopic theory for coupled atomistic magnetization and lattice dynamics, Phys. Rev. Mater. **1**, 074404 (2017).

[17] J. Fransson, Vibrational origin of exchange splitting and chiral-induced spin selectivity, Phys. Rev. B **102**, 235416 (2020).

[18] J. Son, B. C. Park, C. H. Kim, H. Cho, S. Y. Kim, L. J. Sandilands, C. Sohn, J.-G. Park, S. J. Moon, and T. W. Noh, Unconventional spin-phonon coupling via the Dzyaloshinskii-Moriya interaction, npj Quantum Mater. **4**, 17 (2019).

[19] M. C. Weber, M. Guennou, D. M. Evans, C. Toulouse, A. Simonov, Y. Kholina, X. Ma, W. Ren, S. Cao, M. A. Carpenter, B. Dkhil, M. Fiebig, and J. Kreisel, Emerging spin-phonon coupling through cross-talk of two magnetic sublattices, Nat. Commun. **13**, 443 (2022).

[20] H. Katsura, N. Nagaosa, and A. V. Balatsky, Spin Current And Magnetoelectric Effect In Noncollinear Magnets, Phys. Rev. Lett. **95**, 057205 (2005).

[21] M. Mostovoy, Ferroelectricity In Spiral Magnets, Phys. Rev. Lett. **96**, 067601 (2006).

[22] M. Mochizuki, N. Furukawa, and N. Nagaosa, Theory of spin-phonon coupling in multiferroic manganese perovskites RMnO₃, Phys. Rev. B **84**, 144409 (2011).

[23] Y. Ren, C. Xiao, D. Saparov, and Q. Niu, Phonon Magnetic Moment From Electronic Topological Magnetization, Phys. Rev. Lett. **127**, 186403 (2021).

[24] D. Xiao, J. Shi, and Q. Niu, Berry Phase Correction To Electron Density Of States In Solids, Phys. Rev. Lett. **95**, 137204 (2005).

[25] T. Thonhauser, D. Ceresoli, D. Vanderbilt, and R. Resta, Orbital Magnetization In Periodic Insulators, Phys. Rev. Lett. **95**, 137205 (2005).

[26] R. Resta, Electrical polarization and orbital magnetization: The modern theories, J. Phys.: Condens. Matter **22**, 123201 (2010).

[27] R. M. Geilhufe, Dynamic electron-phonon and spin-phonon interactions due to inertia, Phys. Rev. Res. **4**, L012004 (2022).

[28] M. Matsuo, J. Ieda, K. Harii, E. Saitoh, and S. Maekawa, Mechanical generation of spin current by spin-rotation coupling, Phys. Rev. B **87**, 180402(R) (2013).

[29] M. Matsuo, J. Ieda, E. Saitoh, and S. Maekawa, Effects Of Mechanical Rotation On Spin Currents, Phys. Rev. Lett. **106**, 076601 (2011).

[30] M. Matsuo, J. Ieda, E. Saitoh, and S. Maekawa, Spin-dependent inertial force and spin current in accelerating systems, Phys. Rev. B **84**, 104410 (2011).

[31] S. R. Tauchert, M. Volkov, D. Ehberger, D. Kazenwadel, M. Evers, H. Lange, A. Donges, A. Book, W. Kreuzpaintner, U. Nowak *et al.*, Polarized phonons carry angular momentum in ultrafast demagnetization, Nature (London) **602**, 73 (2022).

[32] S. Streib, Difference between angular momentum and pseudoangular momentum, Phys. Rev. B **103**, L100409 (2021).

[33] H. Vogt, Refined treatment of the model of linearly coupled anharmonic oscillators and its application to the temperature dependence of the zone-center soft-mode frequencies of $KTaO_3$ and $SrTiO_3$, Phys. Rev. B **51**, 8046 (1995).

[34] A. S. Barker and J. J. Hopfield, Coupled-optical-phonon-mode theory of the infrared dispersion in $BaTiO_3$, $SrTiO_3$, and $KTaO_3$, Phys. Rev. **135**, A1732 (1964).

[35] M. Kozina, M. Fechner, P. Marsik, T. van Driel, J. M. Glownia, C. Bernhard, M. Radovic, D. Zhu, S. Bonetti, U. Staub, and M. C. Hoffmann, Terahertz-driven phonon upconversion in $SrTiO_3$, Nat. Phys. **15**, 387 (2019).

[36] R. D. King-Smith and D. Vanderbilt, Theory of polarization of crystalline solids, Phys. Rev. B **47**, 1651 (1993).

[37] M. Gajdoš, K. Hummer, G. Kresse, J. Furthmüller, and F. Bechstedt, Linear optical properties in the projector-augmented wave methodology, Phys. Rev. B **73**, 045112 (2006).

[38] G. Kresse and J. Furthmüller, Efficient iterative schemes for *ab initio* total-energy calculations using a plane-wave basis set, Phys. Rev. B **54**, 11169 (1996).

[39] A. Togo and I. Tanaka, First principles phonon calculations in materials science, Scr. Mater. **108**, 1 (2015).

[40] J. P. Perdew, K. Burke, and M. Ernzerhof, Generalized Gradient Approximation Made Simple, Phys. Rev. Lett. **77**, 3865 (1996).

[41] P. Pershan, J. Van der Ziel, and L. Malmstrom, Theoretical discussion of the inverse Faraday effect, Raman scattering, and related phenomena, Phys. Rev. **143**, 574 (1966).

[42] M. Hamada and S. Murakami, Conversion between electron spin and microscopic atomic rotation, Phys. Rev. Res. **2**, 023275 (2020).

[43] I. G. Gurtubay, A. Iturbe-Beristain, and A. Eiguren, Magnetic oscillations induced by phonons in non-magnetic materials, Commun. Phys. **3**, 22 (2020).

[44] X. Li, J. Cheng, J. Cheng, H. Chen, L. Zhang, and J. Zhou, Chiral phonon activated spin seebeck effect, arXiv:2105.08485.

[45] A. V. Podolskiy and P. Vogl, Compact expression for the angular dependence of tight-binding hamiltonian matrix elements, Phys. Rev. B **69**, 233101 (2004).

[46] J. C. Slater and G. F. Koster, Simplified LCAO method for the periodic potential problem, Phys. Rev. **94**, 1498 (1954).

[47] R. M. Geilhufe and W. Hergert, GTPack: A Mathematica group theory package for application in solid-state physics and photonics, Frontiers Phys. **6**, 86 (2018).

[48] W. Hergert and R. M. Geilhufe, *Group Theory in Solid State Physics and Photonics: Problem Solving with Mathematica* (Wiley-VCH, Weinheim, Germany, 2018).

[49] G. E. Jellison, I. Paulauskas, L. A. Boatner, and D. J. Singh, Optical functions of $KTaO_3$ as determined by spectroscopic ellipsometry and comparison with band structure calculations, Phys. Rev. B **74**, 155130 (2006).

[50] M. Choi, F. Oba, and I. Tanaka, Hybrid density functional study of oxygen vacancies in $KTaO_3$ and $NaTaO_3$, Phys. Rev. B **83**, 214107 (2011).

[51] P. Modak and B. Modak, Energetic, electronic, and optical properties of intrinsic charge carrier-trapping defects in $KTaO_3$: Insights from a hybrid DFT study, J. Phys. Chem. C **125**, 24067 (2021).

[52] K. Ueno, S. Nakamura, H. Shimotani, H. Yuan, N. Kimura, T. Nojima, H. Aoki, Y. Iwasa, and M. Kawasaki, Discovery of superconductivity in $KTaO_3$ by electrostatic carrier doping, Nat. Nanotechnol. **6**, 408 (2011).

[53] L. Alber, V. Scalera, V. Unikandanunni, D. Schick, and S. Bonetti, Ntmpy: An open source package for solving coupled parabolic differential equations in the framework of the three-temperature model, Comput. Phys. Commun. **265**, 107990 (2021).

[54] V. Unikandanunni, F. Rigoni, M. C. Hoffmann, P. Vavassori, S. Urazhdin, and S. Bonetti, Ultrafast electron dynamics in platinum and gold thin films driven by optical and terahertz fields, Appl. Phys. Lett. **120**, 021601 (2022).

[55] T. Tsatsoulis, C. Illg, M. Haag, B. Y. Mueller, L. Zhang, and M. Fähnle, Ultrafast demagnetization after femtosecond laser pulses: Transfer of angular momentum from the electronic system to magnetoelastic spin-phonon modes, Phys. Rev. B **93**, 134411 (2016).

[56] B. Koopmans, G. Malinowski, F. Dalla Longa, D. Steiauf, M. Fähnle, T. Roth, M. Cinchetti, and M. Aeschlimann, Explaining the paradoxical diversity of ultrafast laser-induced demagnetization, Nat. Mater. **9**, 259 (2010).